Structure

Article

IspE kinase as an anti-infective target: Role of a hydrophobic pocket in inhibitor binding

Graphical abstract

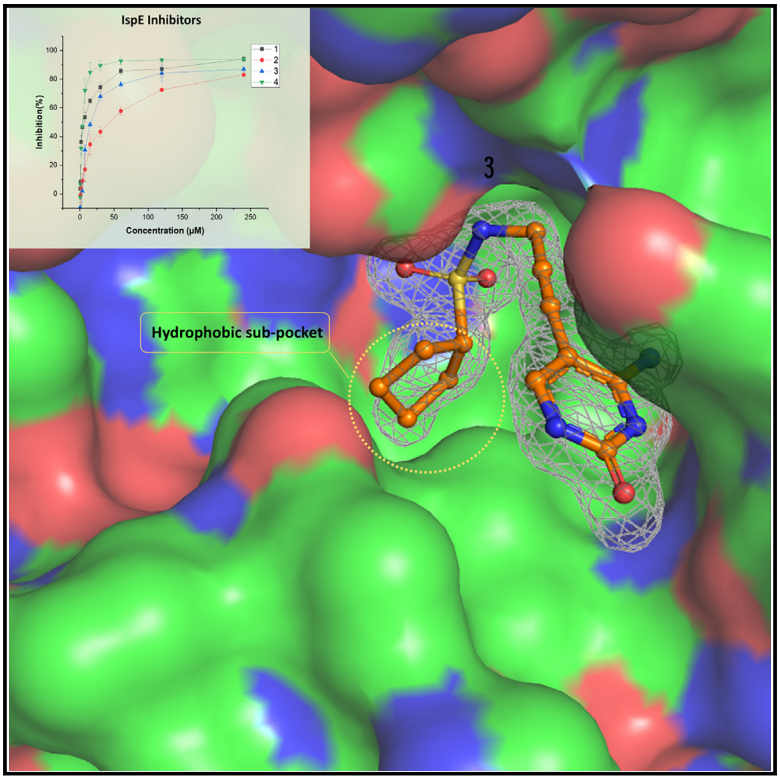

Highlights

- IspE kinase from MEP pathway studied in *E. coli*, *K. pneumoniae*, and *A. baumannii*
- Complex crystal structures reveal distinct inhibitor binding modes in IspE homologs
- *A. baumannii* IspE shows unique inhibitory profile due to tighter hydrophobic subpocket
- Findings guide structure-based design of selective IspE inhibitors for pathogens

Authors

Rawia Hamid, Danica J. Walsh, Eleonora Diamanti, Diana Aguilar, Antoine Lacour, Mostafa M. Hamed, Anna K.H. Hirsch

Correspondence

anna.hirsch@helmholtz-hips.de

In brief

Hamid et al. investigate IspE kinase homologs from pathogenic bacteria, revealing structural differences that necessitate distinct inhibitor strategies. Their findings highlight the importance of the substrate pocket's hydrophobic subpocket for inhibitor design. This study offers valuable insights for developing potent and selective inhibitors targeting the MEP pathway in pathogenic microorganisms.

Hamid et al., 2024, Structure *32*, 1–9
December 5, 2024
https://doi.org/10.1016/j.str.2024.10.009

CellPress

Please cite this article in press as: Hamid et al., IspE kinase as an anti-infective target: Role of a hydrophobic pocket in inhibitor binding, Structure (2024), https://doi.org/10.1016/j.str.2024.10.009

Structure

CellPress
OPEN ACCESS

Article

IspE kinase as an anti-infective target: Role of a hydrophobic pocket in inhibitor binding

Rawia Hamid,[1,2] Danica J. Walsh,[1] Eleonora Diamanti,[1] Diana Aguilar,[1] Antoine Lacour,[1,2] Mostafa M. Hamed,[1] and Anna K.H. Hirsch[1,2,3,*]

[1]Helmholtz Institute for Pharmaceutical Research Saarland (HIPS) – Helmholtz Centre for Infection Research (HZI), Campus Building E8.1, 66123 Saarbrücken, Germany

[2]Department of Pharmacy, Saarland University, 66123 Saarbrücken, Germany

[3]Lead contact

*Correspondence: anna.hirsch@helmholtz-hips.de

https://doi.org/10.1016/j.str.2024.10.009

SUMMARY

Enzymes of the methylerythritol phosphate (MEP) pathway are potential targets for antimicrobial drug discovery. Here, we focus on 4-diphosphocytidyl-2-*C*-methyl-D-erythritol (IspE) kinase from the MEP pathway. We use biochemical and structural biology methods to investigate homologs from pathogenic microorganisms; *Escherichia coli*, *Klebsiella pneumoniae*, and *Acinetobacter baumannii*. We determined the X-ray crystal structures of IspE-inhibitor complexes and studied inhibitors' binding modes targeting the substrate pocket. The experimental results indicate the need for distinct inhibitor strategies due to structural differences among IspE homologs, particularly for *A. baumannii* IspE, which displays a unique inhibitory profile due to a tighter hydrophobic subpocket in the substrate binding site. This study enhances our understanding of the MEP enzymes and sets the stage for structure-based drug design of selective inhibitors to combat pathogenic microorganisms.

INTRODUCTION

There is a growing need for new anti-infectives. The world is racing to identify new microbial targets to combat multidrug-resistant pathogens.[1,2] The 2*C*-methyl-D-erythritol 4-phosphate (MEP) pathway is a rich source of attractive underexplored anti-infective targets[3,4] due to its role in the production of the universal precursors of isoprenoids, especially in pathogenic microorganisms.[5,6] Unlike humans, many of these microorganisms rely on the MEP pathway for the synthesis of the isoprenoids building blocks, isopentenyl diphosphate (IDP) and dimethylallyl diphosphate (DMADP). Several Gram-negative bacteria, like *Escherichia coli*, *Klebsiella pneumoniae*, and *Acinetobacter baumannii* depend on this pathway for isoprenoid production.[7,8] Constituent enzymes of the MEP pathway are validated anti-infective drug targets as confirmed through the *in vivo* efficacy of the antimalarial drug fosmidomycin, which targets the pathway's second step catalyzed by the enzyme IspC.[9,10]

This study focuses on the only kinase present in the MEP pathway, the IspE kinase. The IspE gene (ychB) was first identified in 1999 by Lüttgen et al. as the enzyme that follows IspD in the MEP pathway. They provided evidence of ATP-dependent phosphorylation of the substrate 4-diphosphocytidyl-2-*C*-methyl-D-erythritol (CDP-ME)[11] (Figure 1). Building upon these findings, further investigations led by Kuzuyama and his team, confirmed the role of the ychB gene and provided additional insights into its kinetic product.[12] Until now, IspE crystal structures have been elucidated for *Aquifelix aeolicus* IspE (*Aa*IspE, PDB: 2VF3),[13] *E. coli* IspE (*Ec*IspE, PDB: 10J4),[14] *Thermus thermophilus* (*Tt*IspE, PDB: 1UEK),[15] and *Mycobacterium tuberculosis* (*Mtb*IspE, PDB: 3PYD).[16]

IspE kinase, an ATP-dependent enzyme, shares structural similarities with the galactokinase, homoserine kinase, mevalonate kinase, and phosphomevalonate kinase (GHMP) enzymes. The active site of this family is characterized by five regions responsible for binding the substrate CDP-ME and the co-factor ATP. These regions interact specifically with adenosine, methylerythritol, cytidine, and phosphate groups. Additionally, there is a small hydrophobic pocket that is partially accommodated by the methyl group of the substrate CDP-ME.[13–15] In contrast to most GHMP kinases, IspE is mostly present in solution as a monomer.[17] Two available structures of *E. coli* IspE show two molecules in the asymmetric unit (ASU). Notably, each crystal lattice configuration is distinct. A structure of IspE in complex with CDP-ME and ATP (PDB: 1OJ4) has a 2-fold symmetry.[14] On the other hand, a complex structure of IspE and ADP (PDB: 2WW4), lacks this symmetry, and parts of both molecules in the ASU are found too close to each other's active site, specifically the CDP-ME pocket.[18] This proximity leads to enzyme inactivity *in vivo* because of the unavailable substrate pocket. This suggests that the formation of two molecules in the ASU is a result of the crystallization process itself. This arrangement seems to be predominant in the IspE crystal lattice, which poses a challenge in drug design. Attempting to co-crystallize/soak

Please cite this article in press as: Hamid et al., IspE kinase as an anti-infective target: Role of a hydrophobic pocket in inhibitor binding, Structure (2024), https://doi.org/10.1016/j.str.2024.10.009

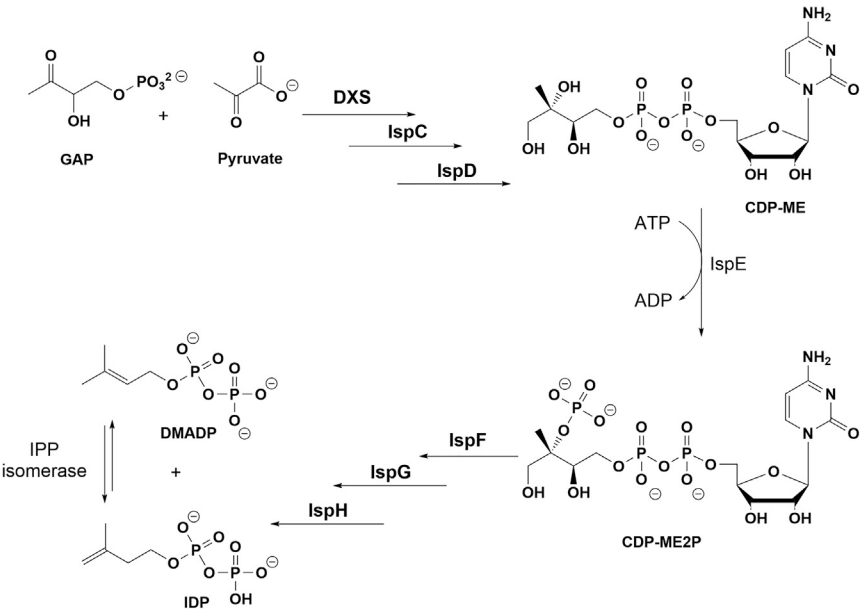

Figure 1. MEP pathway, highlighting the reaction catalyzed by IspE kinase

inhibitors targeting the substrate-binding site to elucidate their binding mode is hampered by an essentially unavailable pocket.

Here we focus on the structural analysis of IspE from human pathogens, namely, *E. coli*, *K. pneumoniae*, and *A. baumannii*. We study the interactions between the ligand and the active site of IspE from these three pathogens. By investigating these aspects, the study seeks to gain a deeper understanding of the IspE enzymes in these human pathogens and their potential as targets for developing new anti-infective agents.

RESULTS AND DISCUSSION

Kinetic characterization of IspE from *E. coli*, *K. pneumoniae*, and *A. baumannii*

To characterize IspE kinase homologs and their inhibitor binding properties, the plasmids containing IspE genes for expressing IspE from *E. coli, K. pneumoniae*, and *A. baumannii* (from BioCat GmbH) were transformed into *E. coli* B21(DE3), the corresponding proteins overexpressed, purified, and their quality analyzed. The activities of the isolated enzymes from the three pathogens were measured by coupling the IspE kinase activity to the auxiliary enzymes lactate dehydrogenase and pyruvate kinase, using a spectrophotometric assay that quantifies the reduction in the absorption of NADH at 340 nm.[19]

E. coli IspE showed a K_m^{CDP-ME} of 200 μM (V_{max} 171 μM min^{-1}) and K_m^{ATP} of 420 μM (V_{max} 195 μM min^{-1}). For *K. pneumoniae* IspE, the apparent K_m^{CDP-ME} was 170 μM (V_{max} 119 μM min^{-1}) and K_m^{ATP} was 348 μM (V_{max} 121 μM min^{-1}). These kinetic values are in the same range as those reported previously.[16,19,20] *E. coli* and *K. pneumoniae* IspE share a sequence homology of 84%, which is also reflected in their kinetic and structural similarity (discussed in the following). *A. baumannii* IspE shows comparable values with a K_m^{ATP} of 474 μM (V_{max} 153 μM min^{-1}); however, it shows slightly higher values of K_m^{CDP-ME}: 358 μM (V_{max} 112 μM min^{-1}) (Figure S1). Noteworthily, *A. baumannii* IspE shares only 39% sequence identity with *E. coli* and 42% with *K. pneumoniae*. Specifically, the sequence alignment from the three homologs reported in Figure S2 highlights the amino acid similarities and differences in the active site that might have contributed to the different patterns of ligand affinities between these homologs. Most prominent are the change of Pro182 in *E. coli* IspE and *K. pneumoniae* IspE into Gln174 in *A. baumannii* IspE, and the change of Cys211 to Phe205 in *A. baumannii* IspE. These two residues are important for binding to the ribose moiety and methyl of the substrate CDP–ME, respectively.

Gel-filtration analysis shows that all three homologs exist mainly as monomers in solution, with a small amount in an oligomeric state (Figure S3). This observation agrees with earlier studies on other IspE kinase homologs and indicates that IspE operates as a monomer, with the active site formed within a single polypeptide unit, without any evident involvement from another subunit in the catalytic process.[13,16,18] The determined biochemical and kinetic values were subsequently used to optimize assay conditions for each homolog to evaluate inhibitory activity.

Molecular structure of *K. pneumoniae* IspE is highly similar to *E. coli* IspE, but crystal packing conceals substrate binding pocket

The 3D structure of *K. pneumoniae* IspE was determined at a resolution of 1.8 Å using molecular replacement and further refined to R-work and R-free values of 19% and 22%, respectively (PDB: 8CKH). *E. coli* and *K. pneumoniae* both belong to the Enterobacteriaceae family, with an 84% sequence identity. Predictably, they show similar structural features reflected in a root-mean-square deviation (RMSD) of 0.557 Å. In addition, conserved residues between the two homologs are involved in binding to ATP and the substrate CDP-ME.

The orthorhombic *K. pneumoniae* IspE crystals contain two molecules in the ASU that bury an interface of 1,167 $Å^2$ by a total solvent-accessible surface area of 24,927 $Å^2$. Strands β2 and β3 and the connecting turn from one molecule point into the substrate binding site of another molecule. This site is occupied by the phosphate of the substrate CDP-ME in the monoclinic crystal form of *E. coli* IspE. The association between the two molecules in *K. pneumoniae* IspE seems to be promoted by a hydrogen bond between the side chain of Arg22 and the main chain of Leu137, with an average distance of 2.8 Å. Such packing of the two molecules prevents substrate or inhibitor binding (Figure 2).

Similar crystallization artifacts have been observed before in the triclinic form of *E. coli* IspE.[18] This observation holds particular significance in drug design, especially when attempting to co-crystallize inhibitors targeting the substrate-binding pocket. In this study, we experimentally show that the structural and

Please cite this article in press as: Hamid et al., IspE kinase as an anti-infective target: Role of a hydrophobic pocket in inhibitor binding, Structure (2024), https://doi.org/10.1016/j.str.2024.10.009

CellPress
OPEN ACCESS

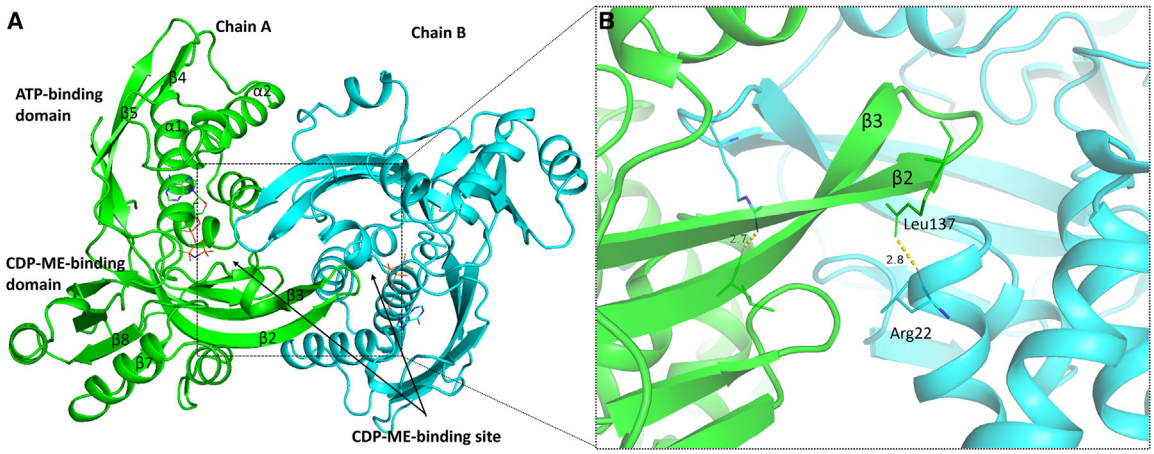

Figure 2. Structure of *Klebsiella pneumoniae* IspE: subunits and domains organization with molecule A shown in green and molecule B in blue

(A) Domain organization: *N*-terminal, ATP-binding domain has four strands and three helices. The ATP binding site is bordering helices 1 and 2. The CDP-ME binding domain is made up of eight strands and five helices in the C-terminal domain. β2 and β3 in the C-terminal domain are antiparallel to each other and they are curved to form the main part of the substrate binding side.

(B) Close-up visualization of the clash the two subunits inflicted on each other where the β2-β3 turn is sliding in the CDP-ME binding pocket. Hydrogen bonds are formed between the Arg22 side chain of one molecule and the main chain in Leu137 of the other molecule (distance 2.8 Å). Interacting residues and ANP are shown as sticks. C: green and yellow; O: red; N: blue; S: yellow.

kinetic values of *K. pneumoniae* IspE prove its high similarity to *E. coli* IspE, suggesting that these two enzymes share a similar way of ligand binding. These findings led to the assumption that they can be used interchangeably for drug-discovery projects, with the recommendation to prioritize the more robust homolog.

Monoclinic structure of *E. coli* IspE: A unique crystal form exhibiting a distinct arrangement of the two subunits that allows ligand binding

The new crystals of *E. coli* IspE found by us align with the overall structure identified for *E. coli* IspE[21] where a similar domain arrangement to the other *E. coli* IspE crystal structure is evident.[14,18] Specifically, the newly found crystals have the space group C2 and diffract at 1.5 Å resolution (refinement statistics can be found in Table S2). In this monoclinic crystal form, the active site pocket is fully accessible for ligand binding as the binding sites of the two subunits were positioned in opposite directions (180° rotation from each other). This configuration created a fully accessible pocket for ligand binding allowing the use of soaking or co-crystallization (Figure 3). We obtained complex structure of *E. coli* IspE with CDP-ME and the unhydrolyzable ATP analog, Adenylyl-imidodiphosphate (ANP), for which a clear density was observed for only two phosphates and not the terminal phosphate, most probably because of the flexibility of the triphosphate. Consequently, we placed ADP in the pocket instead of ANP. The binding of both molecules closely resembles what has been described previously for *E. coli* IspE.[14]

The total solvent-accessible area in the new crystal form is 25.127 Å^2 and the buried interface area is 97.0 Å (3%), compared to 1167.9 Å (23%) in the triclinic structure and 568.7 Å^2 (12%) in the previously reported monoclinic space group *P*21 (calculated using server for Proteins, Interfaces, Structures and Assemblies [PISA]).[22] Figure 3 shows the different crystal forms identified for *E. coli* IspE in comparison to those obtained in this study.

Biochemical evaluation of IspE substrate-competitive inhibitors

In the search for inhibitors against IspE, it is possible either to target the ATP or the substrate-binding sites. Kinase inhibitors are mostly designed to target the ATP-binding site.[23,24] In IspE kinase, however, this pocket is rather shallow and mostly solvent-exposed. Over the years, our group attempted to address this pocket. We, recently, performed a virtual screening on the ATP binding pocket followed by a structure-activity relationship (SAR) study,[25] and in the past Tang et al. used a library of existing GHMP kinase inhibitors.[26] Unfortunately, both attempts were not very successful in developing selective IspE inhibitors targeting the kinase ATP pocket.

On the other hand, the substrate-binding pocket and subpockets have been successfully targeted,[27–29] and the work published in 2007 led to the identification of compound (±)-**1**,[28,30] Figure 4. Brenk's group also extensively focused on the study of IspE inhibitors and they reported *in silico* and high-throughput (HTS) approaches that identified inhibitors in the high micromolar range.[31] It is evident that major efforts are necessary to optimize the existing inhibitors as well as to identify novel hit molecules and, to do so further insights about the binding mode could be very beneficial. Here, we used compound (±)-**1** as a reference inhibitor due to its high potency and selectivity against IspE. As shown in Figure 4, this structure consists of a central cytosine scaffold bearing a tetrahydrothiophene ring, as ribose analogue, bridged via a triple bond to a cyclopropyl sulfonamide. Aiming to identify determinants for IspE inhibition by (±)-**1**, we conducted a focused SAR study that separately targeted each component of the molecule.

The designed and synthesized subset of compounds (**1**—**6**) was simultaneously tested *in vitro* on the three IspE homologs studied in this work (Figure 4). Interestingly, we found that all the compounds showed a similar inhibition pattern against *E. coli* IspE and *K. pneumoniae* IspE, with **5** and **6** being

Please cite this article in press as: Hamid et al., IspE kinase as an anti-infective target: Role of a hydrophobic pocket in inhibitor binding, Structure (2024), https://doi.org/10.1016/j.str.2024.10.009

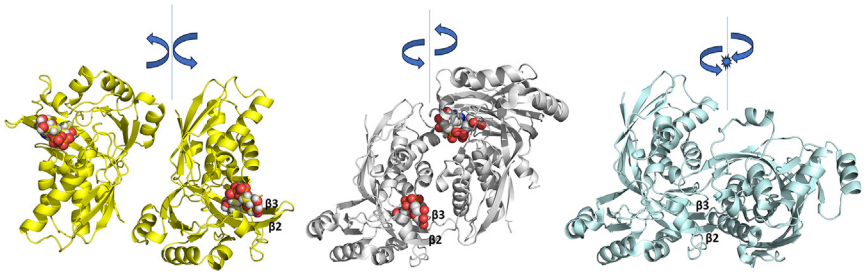

Figure 3. Comparison of *Escherichia coli* IspE crystal conformations in the ASU

Differences between the two monoclinic crystal forms and the triclinic are highlighted. PDB: 8QC7 (monoclinic C121), obtained in this study, is shown in yellow, PDB: 1OJ4 (monoclinic, P 1 21 1) is shown in gray, and PDB: 2WW4 (triclinic P1) is shown in light blue. Molecule A from all crystals is presented in the same orientation to illustrate substrate (CDP-ME, shown as spheres) availability/blockage.

inactive. As expected, the biggest difference is found against *A. baumannii IspE* where only compound **(±)-**1 is still active. The three homologs exhibited an inhibition pattern that correlates with their structural similarities and differences in the binding site, indicating the need for different strategies in designing inhibitors targeting each of these enzyme homologs.

Next, we selected the most potent and soluble compounds for co-crystallization to further confirm their binding mode and guide our optimization strategies. Although we could obtain high-resolution complex structures with *E. coli* IspE, the molecular packing of *K. pneumoniae* IspE prevents substrate and inhibitors designed to bind to the substrate pocket-binding. Nevertheless, due to their high similarity, we propose that the binding mode can be translated from *E. coli* to *K. pneumoniae*. Encouragingly, this assumption is also experimentally supported by the comparable IC_{50} values found. On the other hand, all our efforts have failed in obtaining a complex structure with *A. baumannii* IspE, due to its high solubility, which means that high concentrations are required to drive crystallization. In addition, because *A. baumannii* IspE has

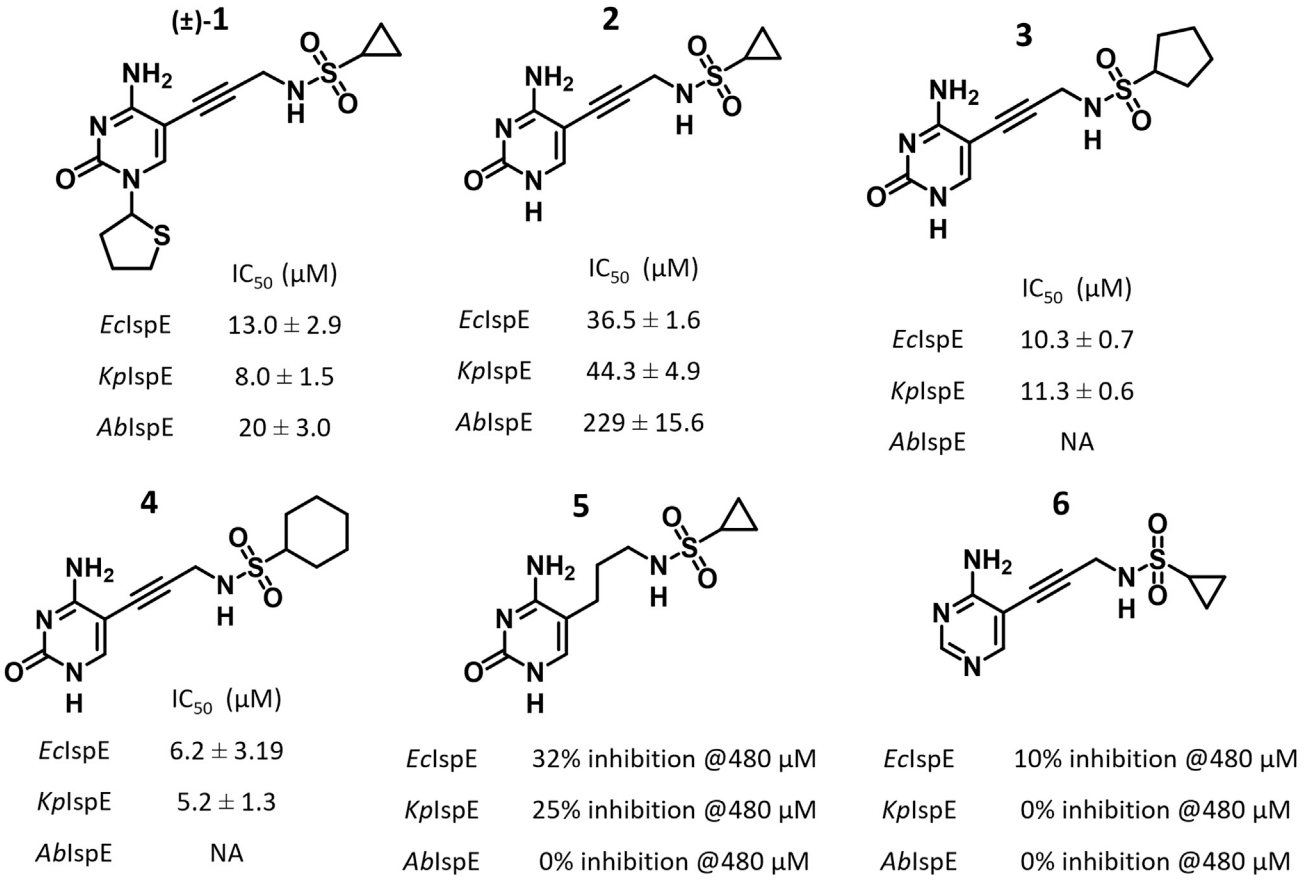

Figure 4. Biochemical evaluation of compounds (1–6)

The half-maximal inhibitory concentration (IC_{50}) on *Escherichia coli* IspE (*Ec*IspE), *Klebsiella pneumoniae* IspE (*Kp*IspE), and *Acinetobacter baumannii* IspE (*Ab*IspE) are depicted. The values presented are average of duplicate measurements. NA: not available; no dose-response curve was obtained to calculate the IC_{50} value.

Please cite this article in press as: Hamid et al., IspE kinase as an anti-infective target: Role of a hydrophobic pocket in inhibitor binding, Structure (2024), https://doi.org/10.1016/j.str.2024.10.009

CellPress
OPEN ACCESS

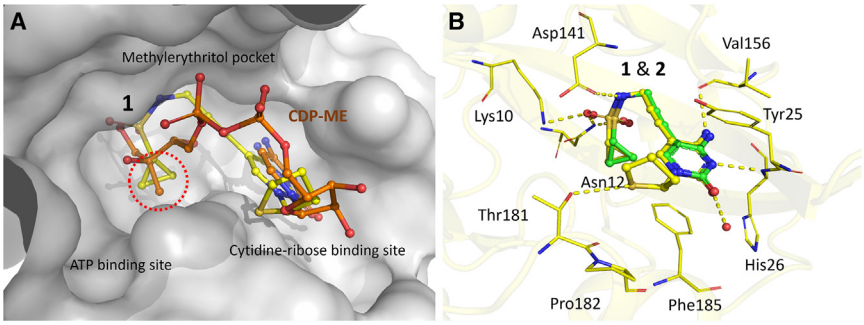

Figure 5. Binding of compound (±)-1 and 2 in the substrate binding site of *Escherichia coli* IspE

(A) Surface representation of *E. coli* IspE active site, showing an overlay between the CDP-ME and the competitive inhibitor **(±)-1** in the substrate pocket. The active site of IspE is composed of three main pockets: the cytidine binding pocket with the ribose sub-pocket, the methylerythritol (ME) binding site featuring a small hydrophobic cavity (highlighted by a red circle), and the ATP binding pocket.

(B) Superimposition of experimental structures of *E. coli* IspE co-crystallized with compounds **(±)1** in yellow and **2** in green showing binding interactions discussed in the text. Molecular surface representations performed using PyMol. Color code: C: green and yellow; O: red; N: blue; S: yellow.

13% lysine residues in its sequence, mostly on the surface, we tried lysine methylation which resulted in poor-quality crystals.

E. coli IspE-inhibitor complex structures

Although the new monoclinic *E. coli* IspE crystals allow soaking experiments, high concentrations of the inhibitor is required in order to exchange the substrate by the inhibitor; therefore, the inhibitors have to be sufficiently soluble. Fortunately, the substrates of the MEP pathway, especially those of the IspE enzyme, are highly polar due to their charged di- and triphosphate groups.[32] As mentioned earlier, for this study our choice was directed toward **(±)-1** and its derivatives. In all the complex structures obtained with *E. coli* IspE and compounds **1** (PDB: 8QCC), **2** (PDB: 8QCN), and **3** (PDB: 8QCO), a consistent interaction pattern was observed. The central cytosine in the inhibitors is positioned between Tyr25 and Phe185, leading to the formation of hydrogen bonds with both the backbone and side chain of His26, similar to the interaction observed with the cytosine ring in CDP-ME, (Figure 5). In the structure with compound **(±)-1,** the tetrahydrothiophene ring overlaps with the ribose moiety of CDP-ME, where it occupies a central position between Tyr25 and Pro182, forming a pseudo-π sandwich (Figure 5A). While these residues are conserved in the *K. pneumoniae* IspE structure, Pro182 is replaced by a Gln174 in *A. baumannii* IspE, which means a different type of interaction will have to take place in this position. Additionally, the sulfur atom of the tetrahydrothiophene ring could potentially point to form hydrogen bonds with either Thr181 or Tyr25. The alkyne linker guides the sulfonamide moiety into the notably polar phosphate binding region situated between the substrate and the ATP binding sites. The nitrogen atom of the sulfonamide forms a hydrogen bond with the side chain of Asp141. Furthermore, the sulfone group, in relation to the NH group, adopts a staggered conformation, facilitating hydrogen bond interactions with the side chain of Asn12 and Lys10. In compounds **1**, **2,** and **3**, the orientation of the cyclopropyl and cyclopentyl rings is directed toward a small hydrophobic pocket delineated by Leu15, Leu28, and Phe32. This hydrophobic region partially contributes to binding the methyl group of the substrate, CDP-ME. Our experimental findings confirm that these compounds are indeed binding to the substrate-binding pocket as intended, forming interactions similar to those observed with the native substrate.

Compound **2** was designed to experimentally evaluate the importance of the tetrahydrothiophene ring. Interestingly, it demonstrated an almost 3-fold decrease in activity with IC_{50} values against *E. coli* IspE and *K. pneumoniae* IspE, and a 10-fold reduction against *A. baumannii* IspE. The complex structure shows that this drop in activity was due to the loss of the tetrahydrothiophene ring's hydrophobic interaction (stacked between Tyr25 and Pro182) and of a potential hydrogen bond of the S atom with Thr181 or Tyr25 (Figure 5B). Despite the dramatic decrease in activity especially against *A. baumannii* IspE, the compound still retained some activity against the other homologs, indicating that the rest of the molecule still significantly contributes to binding.

Aiming to test the optimum binding occupancy of the small hydrophobic pocket, we designed and synthesized compounds **3** and **4** bearing a five and six member ring, respectively, in place of the cyclopropyl of **(±)-1**. The analysis of the co-crystalization with *E. coli* and *K. pneumoniae* IspE showed that both compounds have regained the lost activity in compound **2** and slightly improved the affinity compared to **(±)-1**. Compound **4** with the six-membered cyclohexyl ring further improved the inhibitory activity compared to compound **3** with the five-membered cyclopentyl ring. Theoretical and experimental studies have previously shown that occupation of hydrophobic pockets in a protein target is the main contributor to the binding affinity of the ligand.[33] In IspE, it was found that this hydrophobic pocket, originally accommodating the methyl group of the methylerythritol moiety, is notably more spacious than initially anticipated. Therefore, the appropriate filling of this sub-pocket would result in a significant gain in binding free enthalpy.[34] The volume of this pocket measures roughly around 180 $Å^3$ in *E. coli* IspE and *K. pneumoniae* IspE, while it is only 102 $Å^3$ in *A. baumannii* IspE. Prior studies indicated a significant relationship between its occupancy and activity of the ligands targeting the substrate pocket.[29]

Although we could not obtain a complex structure with compound **4,** due to solubility issues, a co-crystal structure of compound **3** with *E. coli* IspE was obtained, which showed that the cyclopentyl ring indeed occupies the deep hydrophobic pocket surrounded by nonpolar residues, Ile15, Ile17, Leu28, and Ph185 (Figure 6). This hydrophobic interaction exhibited sufficient strength for these two compounds to possess higher affinities than compound **(±)-1**. This factor should be taken into account when considering an extension from this subpocket to the adjacent phosphate-binding pocket.

Please cite this article in press as: Hamid et al., IspE kinase as an anti-infective target: Role of a hydrophobic pocket in inhibitor binding, Structure (2024), https://doi.org/10.1016/j.str.2024.10.009

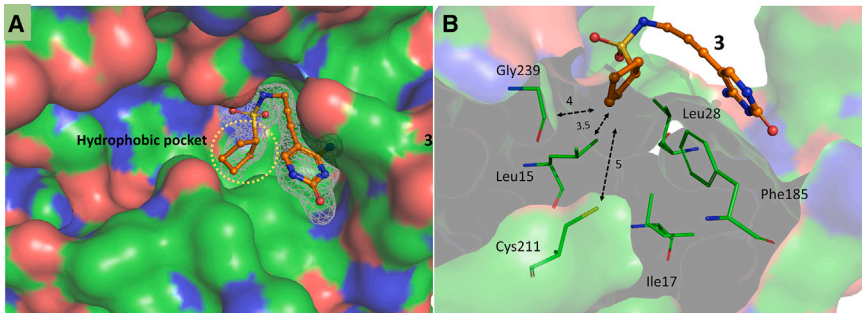

Figure 6. Binding of ligand 3 to *Escherichia coli* IspE (PDB: 8QCO)

(A) Molecular surface representation of *E. coli* IspE showing the hydrophobic pocket occupied by the five-membered hydrocarbon ring from the ligand. (B) Close-up of the small, hydrophobic pocket showing residues of the receptor surrounding the ligand, distance to the closest residues in the hydrophobic pocket are shown in Ångstrom. Color code: C: green; O: red; N: blue; S: yellow.

A. baumannii IspE needs to be targeted using a tailored strategy

Among the subset of compounds synthesized and tested, only **(±)-1** showed inhibition against IspE from *A. baumannii* comparable to the other tested homologs. On the contrary, the inhibition values for **2**, **3,** and **4**, are substantially different. This low activity might also be the reason for the absence of X-ray crystal structure from this homolog. To overcome this bottleneck, we used sequence alignment and homology modeling to rationalize this and to structurally showcase the differences.

The Swiss-Model of *A. baumannii* IspE (Uniprot accession code: B2HUM5) was aligned with the *E. coli* IspE structure in molecular operating environment (MOE) software with an overall RMSD of 1.118 Å.[35,36] Figure 7 shows the structural differences between the two homologs within the CDP-ME binding site.

Compounds **2**–**4** were docked into the CDP-ME binding site of *E. coli* IspE (experimental crystal structure) and *A. baumannii* IspE (Swiss model) resulting in highly similar binding modes. The docking scores are in line with experimental inhibition data showing a slightly lower predicted binding energy of **2** compared with **3** and **4** (Table S2). We attribute this to the reduced ability of the cyclopropyl ring to interact with the small hydrophobic pocket at the back of the binding site.

On the other hand, when looking at Figures 8A–8C, we observe significant differences of the binding mode of these compounds in the *A. baumannii* IspE structure. In particular, for **2** (Figure 8A), there is loss of the interaction of the cytosine carbonyl with His25 as well as the loss of the interaction between the sulfonamide oxygen and the side chain of Asn11 (when compared to the *E. coli* IspE binding mode). Similarly, for **3** (Figure 8B), we observe the loss of hydrogen bonding interactions between the cytosine ring and the backbone of Ile48 with the formation of an internal hydrogen bond instead. Finally, for **4** (Figure 8C), the interactions of the cytosine ring with the backbone are maintained; however, in the docked pose, the sulfonamide no longer interacts with the side chains of Asn11 and Asp133 leading to a loss in predicted binding energy relative to the *E. coli* IspE structure. Taking the inhibition values in mind, there seem to be no side chain movements enough to restore those lost interactions in the *A. baumannii* homolog.

Replacing of the Cys211 in *E. coli* IspE with Phe205 in *A. baumannii* IspE appears to reduce the size of a small hydrophobic pocket. In *E. coli* IspE, this pocket accommodates the cyclopentyl ring of compound **3**. However, the smaller size *in A. baumannii* IspE causes a shift of the compound and a concomitant loss of the important hydrogen bonds with either the cytosine ring or the sulfonamide moiety (Figure 8A). This explains the observed decrease in the experimental activity of these compounds against *A. baumannii* IspE. The replacement of Proline by Glutamine in *A. baumannii* IspE creates an opportunity on the opposite side of the pocket. We can design compounds to form a hydrogen bond with this glutamine residue, potentially improving binding affinity. Furthermore, the 3-membered ring seems optimal for interaction within this pocket. Keeping this core structure while expanding the molecule toward the adjacent ATP binding site could be a promising strategy. This expansion might lead to additional interactions with the protein, potentially improving binding and activity. Combining these approaches, we can potentially develop more potent compounds against *A. baumannii* IspE.

On the other hand, for the homologs from *E. coli* and *K. pneumoniae*, the hydrophobic pocket can be further utilized by incorporating a functional group that forms a covalent bond with the cysteine within the pocket. This stronger interaction could enhance the compound's effectiveness.

A few additional findings are worth mentioning; we tested the importance of the alkyne linker by synthesizing compound **5** with a flexible linker. This resulted in a complete loss of activity across all homologs suggesting the important role of this alkyne linker to direct the cycloalkyl rings into the hydrophobic pocket. The study also highlighted the challenge of cytosine replacement without compromising ligand affinity, a contrast to the numerous adenine substitutions seen in kinase inhibitors. The replacement of cytosine with an amino pyrimidine ring resulted in a significant reduction in activity as observed in compound **6**. It is also worth noting that the most active compound (**4**) has an IC_{50} value of 5.2 μM, leaving room for further optimization. The exclusion of the thiophene ring is a major step in simplifying these derivatives, shortening the synthesis and allowing for higher final yields. These preliminary findings will guide our future development of novel IspE inhibitors.

Conclusions

Our study aimed to characterize IspE kinase homologs, explore the substrate pocket, and study inhibitor binding modes. To achieve this, we recombinantly overexpressed and purified the proteins from *E. coli* IspE, *K. pneumoniae* IspE, and *A. baumannii* IspE; established biochemical assays; and obtained complex structures with inhibitors. While *E. coli* and *K. pneumoniae* IspE exhibited similar kinetics, consistent with previous reports. In addition to showing lower sequence identity, *A. baumannii* IspE kinetic values highlighted its divergence.

Please cite this article in press as: Hamid et al., IspE kinase as an anti-infective target: Role of a hydrophobic pocket in inhibitor binding, Structure (2024), https://doi.org/10.1016/j.str.2024.10.009

CellPress
OPEN ACCESS

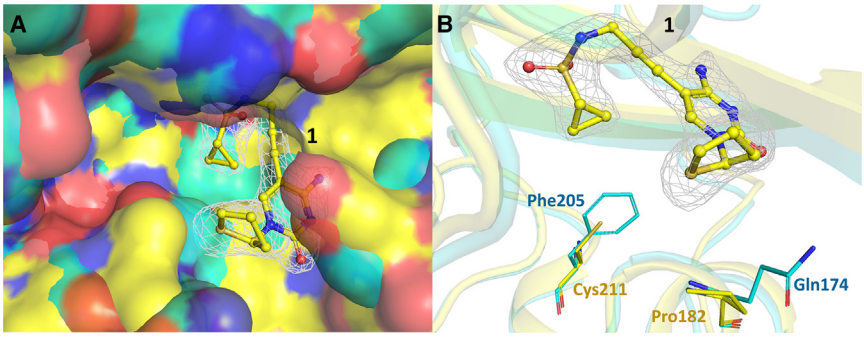

Figure 7. *Escherichia coli* IspE binding to (±) 1 superimposed with homology modeled structure of *Acinetobacter baumannii* IspE

E. coli IspE in yellow superimposed with *A. baumannii* IspE in cyan.

(A) Molecular surface representation of the *A. baumannii* IspE showing the tighter hydrophobic pocket targeted by the cyclopropane in the ligand.

(B) Showing a close-up of the main difference in the active site between the two homologs. In which a cysteine (Cys211) in *E. coli IspE* is replaced by a phenylalanine (Phe205) in *A. baumannii* IspE. Color code: C: cyan and yellow; O: in red; N: in blue; S: yellow.

These values were used in optimizing the assay conditions for each homolog, setting the stage for HTS screening in search of inhibitors.

We presented the crystal structures of *K. pneumoniae* IspE in complex with the non-hydrolysable ATP analog. The 3D-structural characteristics and kinetic parameters of *K. pneumoniae* IspE closely resemble those of *E. coli* IspE. Therefore, we suggest they can be employed interchangeably, particularly when encountering challenges in obtaining and/or crystallizing either enzyme. We identified a new crystalline form for *E. coli* IspE, which allows ligand binding during soaking. We successfully used this condition to obtain three new complex structures of *E. coli* IspE with inhibitors, which allowed us to gain a deeper understanding of the role of methylerythritol hydrophobic subpocket in determining the activity of compounds targeting the substrate binding site. This pocket is relatively bigger in *E. coli* IspE and *K. pneumoniae* IspE and improved compound activity was observed by its proper filling. Covalent targeting of a cysteine residue deep in the pocket might also be considered for further improvements of this compound class. For *A. baumannii* IspE, attention could be drawn to the other side of the pocket where a glutamine replaces a proline, which is important for interaction with CDP-ME and ligands designed to target the substrate pocket.

Our findings emphasize the nuanced nature of IspE kinase inhibition, guided by subtle structural variations among homologs, and offer valuable insights into the development of potent and selective inhibitors for IspE kinase homologs, contributing to the broader goal of combatting pathogenic microorganisms reliant on the MEP pathway.

RESOURCE AVAILABILITY

Lead contact

Further information and requests for resources and reagents should be directed to and will be fulfilled by the lead contact, Anna Hirsch (anna.hirsch@helmholtz-hips.de).

Materials availability

This study did not generate new unique reagents.

Data and code availability

- The electron density maps and their corresponding molecular models have been deposited to the Protein DataBank (PDB) under accession codes PDB: 8CKH, 8QC7, 8QCC, 8QCN, 8QCO and are publicly available as of the date of publication. Accession numbers are also listed in the key resources table. This paper does not report original code. Computational and chemical syntheses are detailed in the supplementary materials. Any additional information required to reanalyze the data reported in this paper is available from the lead contact upon request.

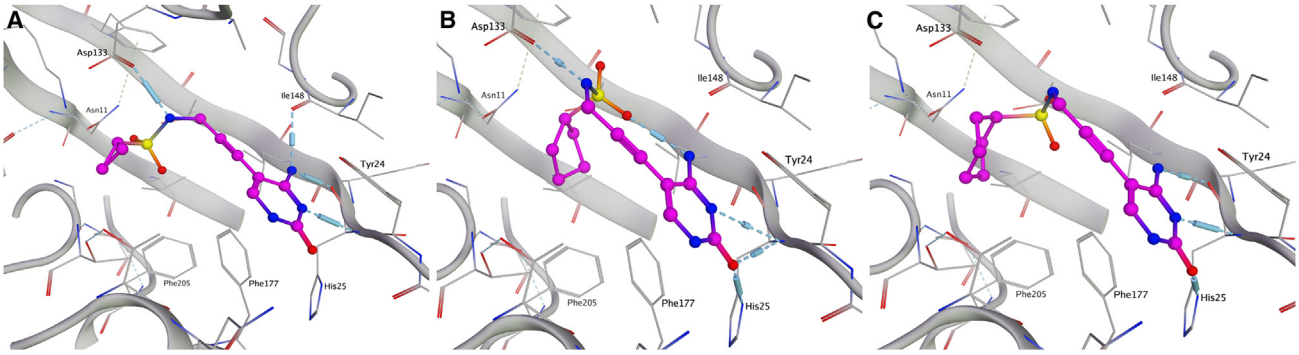

Figure 8. Docking of compounds 2,3 and 4 in *A. baumannii* IspE

(A) Best docked pose of **2** (in magenta) in the *A. baumannii* IspE SwissModel structure (in gray) showing loss of the interaction of the cytosine carbonyl with His25 and the sulfonamide oxygen with the side chain of Asn11.

(B) Best docked pose of **3** (in magenta) in the *A. baumannii* IspE SwissModel structure (in gray) showing loss of hydrogen bonding interactions between the cytosine ring and the backbone of Ile48 and the formation of an internal hydrogen bond instead.

(C) Best docked pose of **4** (in magenta) in the *A. baumannii* IspE SwissModel structure (in gray) showing the shift of the molecule binding, the sulfonamide losses interaction with the side chains of Asn11 and Asp133. Relevant residues are labeled in each picture. Protein residues and ligands shown as sticks, C: gray and magenta; O: red; N: blue; S: yellow.

ACKNOWLEDGMENTS

We acknowledge the European Synchrotron Radiation Facility, Grenoble, France for provision of beamline ID23-1 and ID30B. We acknowledge the Paul Scherrer Institute, Villigen, Switzerland for the provision of synchrotron radiation beamtime at beamline X06DA-PXIII and X06SA-PXI of the SLS.

The authors would also like to thank Boris Illarionov for providing the substrate CDP-ME and Paula Kramer for helping with the computational work.

The Helmholtz Association's Initiative and Networking Fund and the Schlumberger Foundation faculty for the future (FFTF) funded this work.

AUTHOR CONTRIBUTIONS

A.K.H.H. and R.H., conceived the study. R.H. wrote the main manuscript text and prepared all figures. D.J.W. and E.D. synthesized the compounds for bioassays. D.A. performed the bioassay and A.L. performed the docking study. M.M.H. designed and supervised the medicinal chemistry work. All authors proofread the manuscript. A.K.H.H. supervised the project.

DECLARATION OF INTERESTS

The authors declare no competing interests.

DECLARATION OF GENERATIVE AI AND AI-ASSISTED TECHNOLOGIES IN THE WRITING PROCESS

During the preparation of this work the author(s) used ChatGPT-3.5 in order to improve language and readability. After using this tool, the author(s) reviewed and edited the content as needed and take(s) full responsibility for the content of the publication.

STAR★METHODS

Detailed methods are provided in the online version of this paper and include the following:

- KEY RESOURCES TABLE
- EXPERIMENTAL MODEL AND STUDY PARTICIPANT DETAILS
- METHOD DETAILS
  - Enzymatic assays
  - Protein preparation
  - Crystallization
  - Compounds synthesis
  - Computational methods
- QUANTIFICATION AND STATISTICAL ANALYSIS

SUPPLEMENTAL INFORMATION

Supplemental information can be found online at https://doi.org/10.1016/j.str.2024.10.009.

Received: November 20, 2023
Revised: June 24, 2024
Accepted: October 4, 2024
Published: November 6, 2024

REFERENCES

1. World Health Organization (WHO) https://www.who.int.
2. Pulingam, T., Parumasivam, T., Gazzali, A.M., Sulaiman, A.M., Chee, J.Y., Lakshmanan, M., Chin, C.F., and Sudesh, K. (2022). Antimicrobial resistance: Prevalence, economic burden, mechanisms of resistance and strategies to overcome. Eur. J. Pharm. Sci. *170*, 106103. https://doi.org/10.1016/j.ejps.2021.106103.
3. Rohmer, M., Knani, M., Simonin, P., Sutter, B., and Sahm, H. (1993). Isoprenoid biosynthesis in bacteria: a novel pathway for the early steps leading to isopentenyl diphosphate. Biochem. J. *295*, 517–524.
4. Rohmer, M., Seemann, M., Horbach, S., Bringer-Meyer, S., and Sahm, H. (1996). Glyceraldehyde 3-Phosphate and Pyruvate as Precursors of Isoprenic Units in an Alternative Non-mevalonate Pathway for Terpenoid Biosynthesis. J. Am. Chem. Soc. *118*, 2564–2566. https://doi.org/10.1021/ja9538344.
5. Illarionova, V., Kaiser, J., Ostrozhenkova, E., Bacher, A., Fischer, M., Eisenreich, W., and Rohdich, F. (2006). Nonmevalonate Terpene Biosynthesis Enzymes as Antiinfective Drug Targets: Substrate Synthesis and High-Throughput Screening Methods. J. Org. Chem. *71*, 8824–8834. https://doi.org/10.1021/jo061466o.
6. Lange, B.M., Rujan, T., Martin, W., and Croteau, R. (2000). Isoprenoid biosynthesis: The evolution of two ancient and distinct pathways across genomes. Proc. Natl. Acad. Sci. USA *97*, 13172–13177.
7. Gershenzon, J., and Dudareva, N. (2007). The function of terpene natural products in the natural world. Nat. Chem. Biol. *3*, 408–414. https://doi.org/10.1038/nchembio.2007.5.
8. Heuston, S., Begley, M., Gahan, C.G.M., and Hill, C. (2012). Isoprenoid biosynthesis in bacterial pathogens. Microbiol. Read. Engl. *158*, 1389–1401. https://doi.org/10.1099/mic.0.051599-0.
9. Lell, B., Ruangweerayut, R., Wiesner, J., Missinou, M.A., Schindler, A., Baranek, T., Hintz, M., Hutchinson, D., Jomaa, H., and Kremsner, P.G. (2003). Fosmidomycin, a Novel Chemotherapeutic Agent for Malaria. Antimicrob. Agents Chemother. *47*, 735–738. https://doi.org/10.1128/AAC.47.2.735-738.2003.
10. Jomaa, H., Wiesner, J., Sanderbrand, S., Altincicek, B., Weidemeyer, C., Hintz, M., Türbachova, I., Eberl, M., Zeidler, J., Lichtenthaler, H.K., et al. (1999). Inhibitors of the nonmevalonate pathway of isoprenoid biosynthesis as antimalarial drugs. Science *285*, 1573–1576. https://doi.org/10.1126/science.285.5433.1573.
11. Lüttgen, H., Rohdich, F., Herz, S., Wungsintaweekul, J., Hecht, S., Schuhr, C.A., Fellermeier, M., Sagner, S., Zenk, M.H., Bacher, A., and Eisenreich, W. (2000). Biosynthesis of terpenoids: YchB protein of Escherichia coli phosphorylates the 2-hydroxy group of 4-diphosphocytidyl-2C-methyl-d-erythritol. Proc. Natl. Acad. Sci. USA *97*, 1062–1067.
12. Kuzuyama, T., Takagi, M., Kaneda, K., Watanabe, H., Dairi, T., and Seto, H. (2000). Studies on the nonmevalonate pathway: conversion of 4-(cytidine 5′-diphospho)-2-C-methyl-d-erythritol to its 2-phospho derivative by 4-(cytidine 5′-diphospho)-2-C-methyl-d-erythritol kinase. Tetrahedron Lett. *41*, 2925–2928. https://doi.org/10.1016/S0040-4039(00)00295-1.
13. Sgraja, T., Alphey, M.S., Ghilagaber, S., Marquez, R., Robertson, M.N., Hemmings, J.L., Lauw, S., Rohdich, F., Bacher, A., Eisenreich, W., et al. (2008). Characterization of Aquifex aeolicus 4-diphosphocytidyl-2C-methyl-d-erythritol kinase – ligand recognition in a template for antimicrobial drug discovery. FEBS J. *275*, 2779–2794. https://doi.org/10.1111/j.1742-4658.2008.06418.x.
14. Miallau, L., Alphey, M.S., Kemp, L.E., Leonard, G.A., McSweeney, S.M., Hecht, S., Bacher, A., Eisenreich, W., Rohdich, F., and Hunter, W.N. (2003). Biosynthesis of isoprenoids: Crystal structure of 4-diphosphocytidyl-2C-methyl-d-erythritol kinase. Proc. Natl. Acad. Sci. USA *100*, 9173–9178. https://doi.org/10.1073/pnas.1533425100.
15. Wada, T., Kuzuyama, T., Satoh, S., Kuramitsu, S., Yokoyama, S., Unzai, S., Tame, J.R.H., and Park, S.-Y. (2003). Crystal Structure of 4-(Cytidine 5′-diphospho)-2-C-methyl-d-erythritol kinase, an Enzyme in the Non-mevalonate Pathway of Isoprenoid Synthesis. J. Biol. Chem. *278*, 30022–30027. https://doi.org/10.1074/jbc.M304339200.
16. Shan, S., Chen, X., Liu, T., Zhao, H., Rao, Z., and Lou, Z. (2011). Crystal structure of 4-diphosphocytidyl-2-C-methyl-D-erythritol kinase (IspE) from Mycobacterium tuberculosis. FASEB J. *25*, 1577–1584. https://doi.org/10.1096/fj.10-175786.
17. Frank, A., and Groll, M. (2017). The Methylerythritol Phosphate Pathway to Isoprenoids. Chem. Rev. *117*, 5675–5703. https://doi.org/10.1021/acs.chemrev.6b00537.
18. Kalinowska-Tłuścik, J., Miallau, L., Gabrielsen, M., Leonard, G.A., McSweeney, S.M., and Hunter, W.N. (2010). A triclinic crystal form of

Escherichia coli 4-diphosphocytidyl-2 *C* -methyl- D -erythritol kinase and reassessment of the quaternary structure. Acta Crystallograph. Sect. F Struct. Biol. Cryst. Commun. *66*, 237–241. https://doi.org/10.1107/S1744309109054591.

19. Bernal, C., Mendez, E., Terencio, J., Boronat, A., and Imperial, S. (2005). A spectrophotometric assay for the determination of 4-diphosphocytidyl-2-C-methyl-d-erythritol kinase activity. Anal. Biochem. *340*, 245–251. https://doi.org/10.1016/j.ab.2005.01.055.
20. Eoh, H., Narayanasamy, P., Brown, A.C., Parish, T., Brennan, P.J., and Crick, D.C. (2009). Expression and Characterization of Soluble 4-Diphosphocytidyl-2-C-methyl-D-erythritol Kinase from Bacterial Pathogens. Chem. Biol. *16*, 1230–1239. https://doi.org/10.1016/j.chembiol.2009.10.014.
21. Cheek, S., Zhang, H., and Grishin, N.V. (2002). Sequence and structure classification of kinases. J. Mol. Biol. *320*, 855–881. https://doi.org/10.1016/s0022-2836(02)00538-7.
22. Krissinel, E., and Henrick, K. (2007). Inference of Macromolecular Assemblies from Crystalline State. J. Mol. Biol. *372*, 774–797. https://doi.org/10.1016/j.jmb.2007.05.022.
23. Patterson, H., Nibbs, R., McInnes, I., and Siebert, S. (2014). Protein kinase inhibitors in the treatment of inflammatory and autoimmune diseases. Clin. Exp. Immunol. *176*, 1–10. https://doi.org/10.1111/cei.12248.
24. Haveliwala, D.D., Kamdar, N.R., Mistry, P.T., and Patel, S.K. (2014). Chromone-Fused Cytosine Analogues: Synthesis, Biological Activity, and Structure–Activity Relationship. Nucleosides Nucleotides Nucleic Acids *33*, 80–91. https://doi.org/10.1080/15257770.2013.873128.
25. Ropponen, H.-K., Diamanti, E., Johannsen, S., Illarionov, B., Hamid, R., Jaki, M., Sass, P., Fischer, M., Haupenthal, J., and Hirsch, A.K.H. (2023). Exploring the translational gap of a novel class of Escherichia coli IspE inhibitors. ChemMedChem *18*, e202300346. https://doi.org/10.1002/cmdc.202300346.
26. Tang, M., Odejinmi, S.I., Allette, Y.M., Vankayalapati, H., and Lai, K. (2011). Identification of Novel Small Molecule Inhibitors of 4-diphosphocytidyl-2-C-methyl-D-erythritol (CDP-ME) kinase of Gram-negative bacteria. Bioorg. Med. Chem. *19*, 5886–5895. https://doi.org/10.1016/j.bmc.2011.08.012.
27. Hirsch, A.K.H., Alphey, M.S., Lauw, S., Seet, M., Barandun, L., Eisenreich, W., Rohdich, F., Hunter, W.N., Bacher, A., and Diederich, F. (2008). Inhibitors of the kinase IspE: structure–activity relationships and co-crystal structure analysis. Org. Biomol. Chem. *6*, 2719–2730. https://doi.org/10.1039/B804375B.
28. Crane, C.M., Hirsch, A.K.H., Alphey, M.S., Sgraja, T., Lauw, S., Illarionova, V., Rohdich, F., Eisenreich, W., Hunter, W.N., Bacher, A., and Diederich, F. (2008). Synthesis and Characterization of Cytidine Derivatives that Inhibit the Kinase IspE of the Non-Mevalonate Pathway for Isoprenoid Biosynthesis. ChemMedChem *3*, 91–101. https://doi.org/10.1002/cmdc.200700208.
29. Mombelli, P., Le Chapelain, C., Munzinger, N., Joliat, E., Illarionov, B., Schweizer, W.B., Hirsch, A.K.H., Fischer, M., Bacher, A., and Diederich, F. (2013). Imidazole- and Benzimidazole-Based Inhibitors of the Kinase IspE: Targeting the Substrate-Binding Site and the Triphosphate-Binding Loop of the ATP Site: Imidazole- and Benzimidazole-Based Inhibitors of the Kinase IspE. Eur. J. Org. Chem. *2013*, 1068–1079. https://doi.org/10.1002/ejoc.201201467.
30. Hirsch, A.K.H., Lauw, S., Gersbach, P., Schweizer, W.B., Rohdich, F., Eisenreich, W., Bacher, A., and Diederich, F. (2007). Nonphosphate Inhibitors of IspE Protein, a Kinase in the Non-Mevalonate Pathway for Isoprenoid Biosynthesis and a Potential Target for Antimalarial Therapy. ChemMedChem *2*, 806–810. https://doi.org/10.1002/cmdc.200700014.
31. Tidten-Luksch, N., Grimaldi, R., Torrie, L.S., Frearson, J.A., Hunter, W.N., and Brenk, R. (2012). IspE Inhibitors Identified by a Combination of In Silico and In Vitro High-Throughput Screening. PLoS One *7*, e35792. https://doi.org/10.1371/journal.pone.0035792.
32. Persch, E., Dumele, O., and Diederich, F. (2015). Molecular Recognition in Chemical and Biological Systems. Angew. Chem. Int. Ed. *54*, 3290–3327. https://doi.org/10.1002/anie.201408487.
33. Hendsch, Z.S., and Tidor, B. (1994). Do salt bridges stabilize proteins? A continuum electrostatic analysis. Protein Sci. *3*, 211–226.
34. Mecozzi, S., and Rebek Jr, J. (1998). The 55 % Solution: A Formula for Molecular Recognition in the Liquid State. Chem. Eur J. *4*, 1016–1022. https://doi.org/10.1002/(SICI)1521-3765(19980615)4:6<1016::AID-CHEM1016>3.0.CO;2-B.
35. Waterhouse, A., Bertoni, M., Bienert, S., Studer, G., Tauriello, G., Gumienny, R., Heer, F.T., de Beer, T.A.P., Rempfer, C., Bordoli, L., et al. (2018). SWISS-MODEL: homology modelling of protein structures and complexes. Nucleic Acids Res. *46*, W296–W303. https://doi.org/10.1093/nar/gky427.
36. Molecular Operating Environment (MOE) (2022). 02 Chemical Computing Group ULC, 910-1010 Sherbrooke St. W., Montreal, QC H3A 2R7, Canada, 2023..
37. Yuan, S., Chan, H.C.S., Filipek, S., and Vogel, H. (2016). PyMOL and Inkscape Bridge the Data and the Data Visualization. Struct. Lond. Engl. *24*, 2041–2042. https://doi.org/10.1016/j.str.2016.11.012.
38. McCoy, A.J., Grosse-Kunstleve, R.W., Adams, P.D., Winn, M.D., Storoni, L.C., and Read, R.J. (2007). Phaser crystallographic software. J. Appl. Crystallogr. *40*, 658–674. https://doi.org/10.1107/S0021889807021206.
39. Adams, P.D., Afonine, P.V., Bunkóczi, G., Chen, V.B., Davis, I.W., Echols, N., Headd, J.J., Hung, L.-W., Kapral, G.J., Grosse-Kunstleve, R.W., et al. (2010). PHENIX: a comprehensive Python-based system for macromolecular structure solution. Acta Crystallogr. D Biol. Crystallogr. *66*, 213–221. https://doi.org/10.1107/S0907444909052925.
40. Emsley, P., Lohkamp, B., Scott, W.G., and Cowtan, K. (2010). Features and development of Coot. Acta Crystallogr. D Biol. Crystallogr. *66*, 486–501. https://doi.org/10.1107/S0907444910007493.
41. Evans, P.R., and Murshudov, G.N. (2013). How good are my data and what is the resolution? Acta Crystallogr. D Biol. Crystallogr. *69*, 1204–1214. https://doi.org/10.1107/S0907444913000061.
42. Winn, M.D., Ballard, C.C., Cowtan, K.D., Dodson, E.J., Emsley, P., Evans, P.R., Keegan, R.M., Krissinel, E.B., Leslie, A.G.W., McCoy, A., et al. (2011). Overview of the CCP4 suite and current developments. Acta Crystallogr. D Biol. Crystallogr. *67*, 235–242. https://doi.org/10.1107/S0907444910045749.

Please cite this article in press as: Hamid et al., IspE kinase as an anti-infective target: Role of a hydrophobic pocket in inhibitor binding, Structure (2024), https://doi.org/10.1016/j.str.2024.10.009

STAR★METHODS

KEY RESOURCES TABLE

REAGENT or RESOURCE	SOURCE	IDENTIFIER
Chemicals, peptides, and recombinant proteins		
LB-Medium	Roth	6669.3
Kanamycin	Roth	T832.3
TEV Protease	Biolabs	P8112S
ATP	Sigma Aldrich	A2383
NeXtal Crystallization Kits	Qiagen	130704, 130716, 130701
Deposited data		
K. pneumoniae IspE	This paper	PDB: 8CKH
E. coli IspE (CDP-ME)	This paper	PDB: 8QC7
E. coli IspE (Ligand 1)	This paper	PDB: 8QCC
E. coli IspE (Ligand 2)	This paper	PDB: 8QCN
E. coli IspE (Ligand 3)	This paper	PDB: 8QCO
Recombinant DNA		
pET-28a (+) *E.coli* IspE	BioCat	729915–1
pET-28a (+) *K. pneumoniae* IspE	BioCat	719980–1
pET-28a (+) *A. baumannii* IspE	BioCat	721316–1
Software and algorithms		
OriginPro2023 (10.0.0.0.154)	OriginLab	www.originlab.com
MOE (v2022.09)	Chemical Computing Group	www.chemcomp.com
PyMoL (2.5.5)	Schrödinger[37]	pymol.org
Phenix (1.20.1–4487)	Phenix Software LLC[38,39]	phenix-online.org
Coot (0.9.4.1)	Coot[40]	www2.mrc-lmb.cam.ac.uk
Other		
ÄKTA Pure System	Cytiva	29018224
S200 SEC Column	Cytiva	28990944
HisTrap HP 5 mL column	GE Healthcare	17524801

EXPERIMENTAL MODEL AND STUDY PARTICIPANT DETAILS

This study used *E. coli* BL21 (DE3) as an overexpression host strain, Internal code: H083.

METHOD DETAILS

Enzymatic assays

Assay setup

A coupled spectrophotometric enzyme assay was used to measure IspE activity and kinetic parameters at room temperature over 30 min. IspE concentrations were 200 nM for *E. coli*, 150 nM for *K. pneumoniae*, and 100 nM for *A. baumannii*. Kinetic assays were performed with varying ATP and CDP-ME concentrations, with one held constant (1 mM ATP or 2 mM CDP-ME). IC_{50} values for inhibitors were calculated from linear curves of initial velocities using nonlinear regression analysis (OriginPro2023) (Figure S1).

Protein preparation

Transformation and culture

Plasmids containing the IspE constructs for *E. coli*, *K. pneumoniae*, and *A. baumannii* were transformed into electrocompetent *E. coli* BL21 (DE3) cells. Transformants were cultured on LB-Agar plates supplemented with 25 μg/mL kanamycin and incubated overnight

Please cite this article in press as: Hamid et al., IspE kinase as an anti-infective target: Role of a hydrophobic pocket in inhibitor binding, Structure (2024), https://doi.org/10.1016/j.str.2024.10.009

at 37°C. Single colonies were transferred into LB medium with 25 μg/mL kanamycin and cultured at 37°C. The cultures were grown until an OD600 of 0.3–0.6 for *E. coli* and *K. pneumoniae* IspE, and 0.8 for *A. baumannii* IspE. Protein overexpression was induced with 1 mM IPTG at 18°C with shaking at 180 RPM overnight.

Protein purification

Cells were harvested by centrifugation, resuspended in 50 mM Tris-HCl (pH 7.5), 200 mM NaCl, and lysed using Microfluidizer. Lysates were purified using a HisTrap HP 5 mL column, washing buffer; 50 mM Tris-HCl (pH 7.5), 200 mM NaCl, 20 mM Imidazole, elution buffer; 50 mM Tris-HCl (pH 7.5), 200 mM NaCl, 300 mM Imidazole. His-tags were cleaved by incubation with TEV protease at a ratio of 1:20 (protease: protein). The cleavage mixture was passed through a reverse IMAC column to remove cleaved tags and uncut protein. Tag-free proteins were further purified using an ÄKTA pure system with an S200 column. Peak fractions were collected, concentrated, and stored in 20 mM Tris-HCl (pH 7.5), 200 mM NaCl. SDS-PAGE was used to assess the purity of the IspE homologs at each purification step (Figure S3).

Gel filtration analysis

A gel filtration column was calibrated with standard proteins ranging from 670 kDa to 1.35 kDa. A defined volume of the purified IspE sample was injected into the calibrated column. Protein elution was monitored using UV detection at 280 nm, and the elution profile was compared to standards to estimate the molecular weight of *IspE*. A calibration curve was constructed (Figure S3).

Crystallization

Screening and optimization

Crystallization conditions were screened using NeXtal crystal screening kits and incubated at 18°C. Optimization was performed based on initial hits.

Specific conditions

***K. pneumoniae* IspE:** Crystallized from 15 mg/mL protein with 5 mM AMP-PNP, CDP-ME, and MgCl2 in vapor diffusion chambers with 1000 mM Sodium citrate and 100 mM HEPES pH 7.0. ***E. coli* IspE:** Crystallized from 7.5 mg/mL protein in 25% PEG 4k, 200 mM MgCl2, and 100 mM MES pH 6.5. Crystals were soaked with 5–10 mM compounds for 2 days.

X-Ray data collection and structure determination

Crystals were cryoprotected with 32% glycerol and data collection was carried out at SLS and ESRF beamlines. Structures were determined by molecular replacement using Phaser.MR in Phenix,[38,39] with *E. coli* IspE (PDB ID: 1OJ4) as the model. Data were reduced and aligned using AIMLESS[41] in CCP4i,[42] with manual map interpretation in COOT.[40] Iterative refinement was performed with Phenix refine, followed by validation on the PDB server. Figures were generated using PyMoL (Figure S2).

Compounds synthesis

Commercially sourced chemicals were used without further purification. TLC monitored reaction progress, and column chromatography was performed using a CombiFlash Rf system. RP-HPLC was performed on a Thermo Fisher UltiMate 3000 system. 1H and 13C NMR spectra were recorded on Bruker instruments. LCMS purity checks were conducted on an Ultimate 3000-MSQ system. Compounds used in assays had $\geq$95% purity, and high-resolution mass spectra were obtained on a Q Exactive Focus system (Data S1 and Methods S1).

Computational methods

Molecular docking for IspE inhibitors was performed using MOE v2022.09. Ligands were energy minimized, and protein structures prepared with force fields and hydrogen assignment. Docking was conducted using the Dock module with scoring functions applied to assess results. Detailed methods are in the supplementary materials (Methods S2).

QUANTIFICATION AND STATISTICAL ANALYSIS

Enzyme kinetics and IC_{50} values were calculated using nonlinear regression analysis in OriginPro2023. Calibration curves for gel filtration were constructed using standard proteins. Crystallization and structural analysis methods followed standard protocols as referenced. X-ray crystallography data collection and refinement statistics are summarized in Table S1.